Investigating responses of calcium carbonate nucleation rates in artificial seawater to changes in saturation states due to ocean acidification

Daniel Anderson[1]

Advisor: Alex Gagnon

[1]University of Washington, School of Oceanography, Box 357940, Seattle, Washington, 98195-7940

anderd8@uw.edu

16 May 2016

Abstract:

Reduced saturation states of carbonate ions caused by ocean acidification make it harder for marine calcifiers such as corals to build their shell or skeleton. Nucleation is vital to corals because it is a necessary precursor to the crystal growth that builds coral skeletons. This study examines changes in inorganic calcite nucleation rates over different carbonate saturation states as a first step to understanding aragonite nucleation and predicting how coral growth is affected by changes in acidity. To accomplish this, a temperature-controlled microscope flow-cell is used with time-lapse photography to compare nuclei densities at different saturation states. Inorganic calcite nucleation rates are sensitive to carbonate saturation states based on nucleation pathways and classical nucleation theory. These results extend existing data to low saturation states, which are considered to be more in the physiological realm of nucleation.

Introduction:

Anthropogenic carbon dioxide added to the atmosphere has increased carbon dioxide concentrations by a third, from pre-industrial levels of about 300 parts per million by volume (ppmv) to over 400 ppmv today, which has reduced pH levels by 0.1-0.2 units in the average global surface waters (IPCC 2014). Increasing anthropogenic carbon dioxide emissions have been linked to warming oceans, ocean acidification, and higher UV radiation (Doney et al. 2012; Crutzen P.J. 1992). Atmospheric concentrations would be about 450 ppmv if oceans did not absorb approximately a third of the atmospheric carbon (Sabine & Feely 2007, Sabine et al. 2004).

Eq 1: $CO_{2(aq)} + CO_3^{2-}{}_{(aq)} + H_2O_{(l)} \rightarrow 2HCO_3^-{}_{(aq)}$

Eq 2: $Ca^{2+}{}_{(aq)} + CO_3^{2-}{}_{(aq)} \rightarrow CaCO_{3(s)}$

Eq 3: $\Omega = ([Ca^{2+}][CO_3^{2-}]) / K_{sp}$

DIC or $C_t = [CO_2^*] + [HCO_3^-] + [CO_3^{2-}]$

Figure 1: General chemical equations for carbonate chemistry in seawater.

The process of ocean acidification occurs when excess carbon dioxide dissolves into the ocean to combine with a carbonate ion and a water molecule to form two bicarbonate ions as seen in Equation 1 in Figure 1(Doney et al. 2009). This acidification process decreases pH and removes carbonate ions from the water column. By the end of the century, it is predicted that pH levels will decrease by another 0.3-0.4, which is equivalent to a 150% increase in hydrogen ions and a 50% decrease in carbonate ions (Orr et al. 2005). This carbonate reduction will have negative effects on corals such as being unable to produce their skeleton and losing their structural support and protection (Doney S.C. 2010; Hoegh-Guldberg, O. & Bruno, J.F. 2010). Corals are marine calcifiers and use calcium and carbonate ions from the water column to create their skeleton as seen in Equation 2 of Figure 1 (Doney et al. 2009). The saturation state or Ω is defined as the amount of ion reactants, calcium and carbonate, divided by the solubility constant. Corals are found around the world's oceans in a variety of skeletal structures important for reef structure, coastal protection, fish habitat, and ecotourism. Unfortunately, these organisms are also known for being affected by ocean acidification.

Corals utilize biomineralization to create their calcium carbonate skeleton by creating a thin organic layer over the growth site or calcifying space at the base of

each polyp's gastric cavity or coelenteron (Allemond, D. et al. 2004). Biomineralization is a process corals use to biologically regulate the area where the skeleton forms on a molecular level (Meldrum, F.C. 2003). Previous work has shown that calcium carbonate will preferentially nucleate on unique templates during inorganic experiments. Presumably, similar interactions control shape and density of coral skeletons as part of biomineralization (De Yoreo, J.J. & Vekilov, P.G. 2003). Corals pump certain ions through their organic layer to regulate ionic strength, pH, and impurity content (De Yoreo, J.J. & Vekilov, P.G. 2003). One study by Venn et al. (2012) first used boron isotopes and then confocal microscopy with fluorescent probes to find pH was regulated at the calcifying space. They also found that the difference between the environmental solution and the calcifying fluid became greater when acidified, but the saturation state of the calcifying fluid still decreased with ocean acidification. Cai et al. (2016), used microelectrode inserted directly into the coelenteron to measure pH and DIC through the gastric cavity and in to the calcifying fluid. The group found that for the corals, *Orbicella faveolata, Turbnaria reniformis* and *Acropora millipora*, the pH spiked dramatically when the microelectrode reached the calcifying fluid while the DIC stayed at similar levels. These results reinforce previous work done with microelectrodes on Galaxea *fascicularis* and *Astrangia poculata* that demonstrated the spike in pH but did not measure the DIC through the coelenteron (Al-Horani et al. 2003; Ries, J.B. 2011). The dramatic increase in pH while DIC remains constant by a proton pump leads to a very high aragonite saturation state with an omega range of 8-22 with less energetic requirements (Cai et al 2016). This biologically regulated high saturation

state is a critical constituent corals use in biomineralization to assist with nucleation and crystal growth by reducing thermodynamic energy barriers. Although corals can influence the saturation state in the calcifying fluid through biomineralization, the process of nucleation is still sensitive to ocean acidification.

Aragonite nucleation is a crucial step in the biomineralization of coral skeletons, so it is vital to understand its energetic mechanisms in order to predict how nucleation rates will change in future marine environments. Nucleation continuously occurs while the coral grows its skeleton (Gladfelter, E.H., 1982). From inorganic experiments, these rates are usually interpreted using Classical Nucleation Theory, which provides rough predictions of nucleation rates based on critical factors such as saturation states and interfacial free energy, which is the free energy of the surface of the nuclei. Due to a change in interfacial free energy, nuclei are unstable until the critical size is reached where the volume to surface ratio is large enough to overcome the Gibbs-Thompson effect and become stable (De Yoreo, J.J. & Vekilov, P.G. 2003). Nucleation can occur either in solution or on a surface, which implies that there are two interfacial energies to consider, and both have different thermodynamic barriers to nucleation that have to be overcome by some driving force (De Yoreo, J.J. & Vekilov, P.G. 2003). A sufficiently high saturation state is commonly used, where saturation state is a measure of the thermodynamic driving force for mineral growth and is defined as the ratio of ion activities in solution over the solubility product as seen in Equation 3 in Figure 1. Calcium carbonate, formed from calcium and carbonate ions in solution (Equation 2 in Figure 1), is found in five known polymorphs with calcite being most stable and

amorphous calcium carbonate (ACC) being highly unstable. The aragonite polymorph is less stable than calcite in solution, but magnesium ions have been found to restrict calcite from nucleating, thus allowing aragonite to form instead (Berner, R.A. 1975). When carbonate ions are removed by ocean acidification, the aragonite saturation state, or omega value, is reduced from Equation 3 in Figure 1 and the thermodynamic barrier is increased. Although corals use aragonite to form their skeleton, the polymorph of calcite can be precipitated using simpler solutions and while some properties are different, investigating calcite nucleation rates can be used as a stepping stone to understanding how aragonite nucleation will be affected by saturation states in the future.

There are various approaches to change or reduce energy barriers for each case of nucleation, but little work has been done to quantify the importance of changes in saturation due to pH for calcium carbonate nucleation. In a study by Hamm et al. (2014), a flow-cell was used with a volume of 0.5mL and a total flow rate of 1ml per minute to discern calcite nucleation on a variety of chemically altered surfaces with different organic functional groups. Nucleation rates of calcite decreased exponentially with a reduction in carbonate saturation states (Hamm et al. 2014). However, in the experiments done by Hamm et al. (2014), the saturation states were kept very high in order to see amorphous calcium carbonate form as well as calcite. It is important to test if these data would apply to lower saturation states for a more physiologically relevant result. It can be assumed that aragonite nucleation rates will have a similar response as calcite due to similarities in size and dynamics in the Classical Nucleation Theory. A similar study was also performed

with kinetics of silicate nucleation and different surface interfacial energies (Wallace et al. 2009). Wallace et al. (2009) found silica nucleation rates and subsequent energy barriers varied by magnitudes for six different carboxyl- and anime- terminated surfaces. Changing the interfacial surface energy can have a large impact on nucleation rates of silica, making it important to understand how surfaces used in this experiment affected the nucleation energy barrier. Hu et al. (2012) also looked at interfacial surface energies, but with calcite, and found similar surfaces that reduced the energy barrier to nucleation. Although scientists have investigated some of the manipulations to the thermodynamic barriers of nucleation for silica and calcite, there has been little work to quantify how the saturation state can affect aragonite nucleation rates or calcite nucleation rates with lower saturation states.

This project begins to fill the gap in scientific knowledge of inorganic calcium carbonate nucleation by quantifying and explaining changes in rate of inorganic calcite nucleation in response to differing saturation states of carbonate ions. Understanding the fundamentals of calcium carbonate nucleation has the potential to revolutionize how scientists view the future of hard corals, or corals that secrete an aragonite skeleton. An increase in energy required for calcification could cause an energy loss in other areas such as growth and reproduction (Doney et al. 2012; Pandolfi et al. 2011). Hard corals are the backbone for coral reef ecosystems in that they provide the majority of the structure, food, and protection (Pandolfi et al. 2011). These essential coral reefs will face an increased threat from ocean acidification, while also dealing with increasing water temperature and increases in the frequency and strength of storms (Orr et al. 2005). Loss of coral reefs is

devastating as they provide billions of dollars worth of goods and services for local and commercial fisheries, ecotourism, and the production of future medical cures (Costanza et al., 1997; Johns et al., 2001; Jameson et al., 1995). In an effort to better predict and hopefully avoid this impact, the results of this project will help scientists better understand how coral's calcium carbonate nucleation will be affected by a decline in future carbonate saturation levels by providing inorganic nucleation rates for changing calcium carbonate saturation states.

Methods:

Approach:

A successful experiment requires recognition and control of several parameters to collect inorganic calcium carbonate nucleation data. In order to view calcium carbonate nucleation densities, a temperature-controlled microscope flow-cell was designed, engineered, and constructed (Figure 3 & 4). The temperature had to be controlled as it can change nucleation rates. Also, the main thermodynamic driving force used to control nucleation rate will be saturation state. Therefore, concentrations of calcium and carbonate ions have to be well maintained which includes manipulation of pH. Two solutions, with dissolved inorganic carbon (DIC) in one and calcium ions in the other, were mixed separately in low-density polyethylene or LDPE bottles and then pumped at equivalent rates through the mixing chamber where the reaction initiates and then into the flow-cell to ensure that nucleation occurred in the viewing chamber. The polymorph of calcium carbonate forming on the glass slide can be identified with confidence using Raman

spectroscopy. For each experimental run at a different saturation states, the densities of calcium carbonate nuclei were counted using a computer-controlled microscope. Rates of inorganic calcium carbonate nucleation were compared to saturation states in the flow-cell.

Solution Chemistry:

The different saturation states were achieved by creating two separate solutions: one with the calcium component and the other with the DIC and Alkalinity component. This was done by massing out calcium chloride into an LDPE bottle (Bottle Ca^{2+}) for the calcium component and sodium bicarbonate and sodium hydroxide into the other LDPE bottle (Bottle DIC) for the DIC component. The LDPE bottles were both filled with milli-q water and massed for a final time after being thoroughly mixed. The concentrations for the final solution were kept similar to seawater and thus sodium chloride was added to each bottle at a concentration of 0.45M. The calcium concentration was also kept constant at 0.01M for the combination of the two solutions in each experimental run. The amount of sodium hydroxide varied for each experimental run, which manipulated pH and the carbonate ion saturation state. By using DIC equations, the masses of the compounds added, and by keeping the DIC constant at 0.002M, the saturation state or omega was calculated for each run. Each experimental run had a different saturation state in order to evaluate the impact of omega on rates of aragonite nucleation.

Using the alkalinity titrator and DIC coulometer, actual values of Total Alkalinity (TAlk) and DIC were measured for select experimental runs and

compared with calculations. These values were used to determine if the solutions were close to desired concentrations of calcium and DIC. The creation of the solutions was eliminated as a point of error because the experimental values were determined consistent with theoretical values with a 36.31 μmol/kg (1.7%) increase in DIC from the target and a 55.59 μmol/kg (2.3%) increase in Total Alkalinity. The DIC and TAlk are both expected to increase by a small amount due to the salt absorbing water while weighing. However, when DIC increases, the saturation state will decrease, and when TAlk increases, the saturation state will increase. In the end, the saturation state stayed within a value of 0.1 units.

The solutions were then moved from the LDPE bottles to two airtight bags to limit and prevent further atmospheric carbon exchange, and then kept at 25 degrees Celsius, which was chosen because it is similar to average temperature of coral reefs and close to room temperature. A peristaltic pump allowed for continuous and simultaneous flow of the calcium and DIC solutions from the gas-bags to the mixing chamber. The mixing chamber was a 30ml LDPE bottle with two 3-inch input Tygon tubes on the bottom and one 3-inch exit Tygon tube coming out of the lid (Figure 2). A magnetic stir bar is added and the container is sealed and placed on a stir plate. The mixing chamber allows the solution to have constant chemistry before entering the flow-cell.

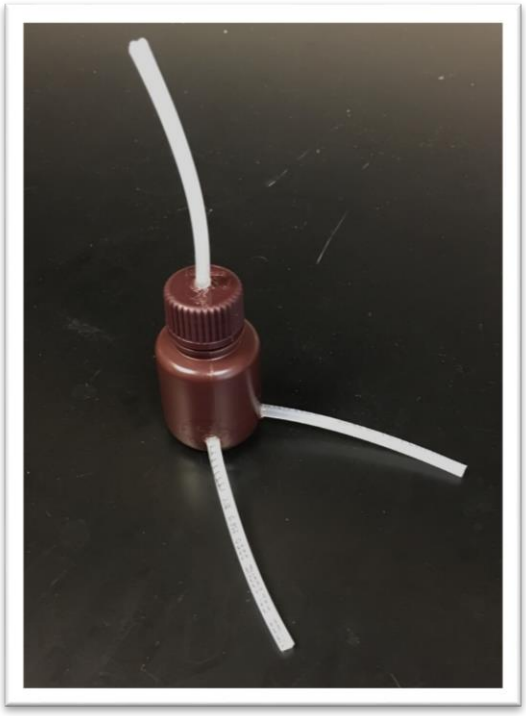

Figure 2: Mixing chamber constructed with 1mm ID Tygon tubing attached to a 30 mL LDPE bottle with a small stir bar inside.

Flow-Cell:

The mixed solution then entered the aluminum flow-cell with a viewing chamber made by glass microscope slides sealed with an O-ring and two plastic plates that press the glass against the O-ring. Aluminum was used as the base material for the flow-cell because of its high heat conductivity. Pipes were drilled down the sides of the flow-cell to allow coolant to flow through the cell and provide a constant temperature. The flow-cell was then set onto a base plate, which can be mechanically attached on to the microscope stage (Figure 3&4). The entire apparatus was designed to be only 14mm thick to fit under the microscope objectives. By using this set-up, calcium carbonate nucleation can be viewed through a microscope. The nucleation on the top slide of the flow-cell is used for measuring nucleation rates because the calcium carbonate can nucleate and fall out of solution onto the bottom slide. In order to keep the saturation state similar

throughout the chamber, a mixing blockade was fashioned and added to the beginning of the chamber. A fine mesh stainless steel screen was used as the mixing blockade and placed 8mm after the input. The mixing in the flow-cell was tracked by pumping low concentrations of fluorescein dye through the viewing chamber at different flow rates and with different mixing blockades. By using fluorescein dye experiments, the screen was found to be the best type of mixing blockade to create a laminar flow through the flow-cell. After numerous flow-cell tests and the fluorescein dye experiments, a flow rate of 3 ml/min per solution was chosen to balance the residence time inside the viewing chamber with the time spent in the mixing chamber while keeping the saturation state constant after calcium carbonate has nucleated out of the previous solution. At this flow rate, the residence time in the mixing chamber is 5 minutes to allow nucleation to happen with fresh solution without turbulence being a problem.

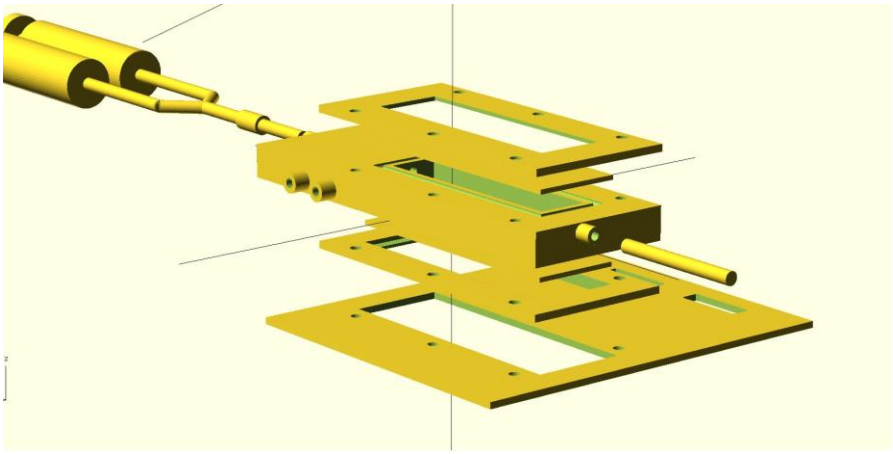

Figure 3: External CAD model of the temperature-controlled microscope flow-cell.

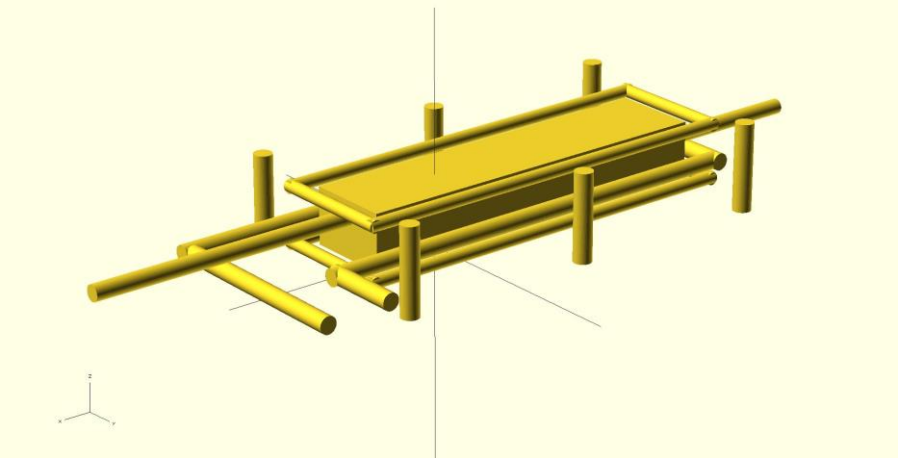

Figure 4: Internal CAD model of the temperature-controlled microscope flow-cell. The vertical columns are bolt holes, the top and bottom rectangle are cut for an O-ring, and the middle pipe is made for the coolant fluid.

Crystals:

After several nucleation trials in the flow cell, there were a couple of polymorphs of calcium carbonate that formed with unique structures. In order to be sure of what polymorph was forming on the flow-cell slide, Raman Spectroscopy was used to identify and confirm what crystal was formed (Figure 5 & 6). Raman Spectroscopy is used by looking at how the bonds within a crystal interact with a beam of light at a specific wavelength. Each polymorph of calcium carbonate has a distinctive signature. Raman Spectroscopy was used instead of X-ray diffraction because of the ability to focus the laser on a specific nuclei or crystal. The spectra were identified using excitation at a wavelength (λ) of 514nm. Raman spectrum standards were found from aragonite and calcite in mineral collections with the mineralogy independently confirmed by powdered X-ray diffraction. Although most of the peaks of intensity are very similar between calcite and aragonite, there is a

clear distinction between the aragonite peak at 212 and the calcite peak at 284. This distinction made it obvious what polymorph was nucleating on the glass slide in the flow-cell.

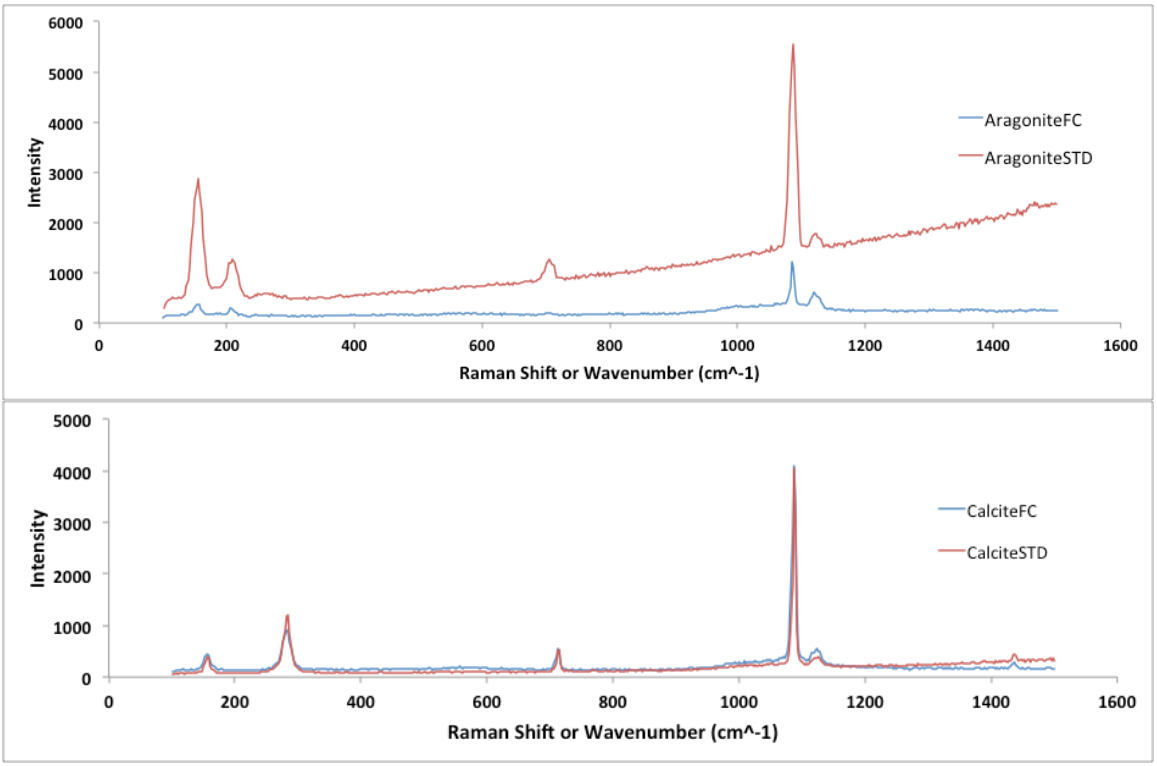

Figure 5: A Raman spectrum of crystals formed in the flow cell during experimental runs. The peaks from left to right for the aragonite spectrum are as follows: 155, 212, 707, and 1087. The peaks from left to right for the calcite spectrum are as follows: 158, 284, 715, and 1087.

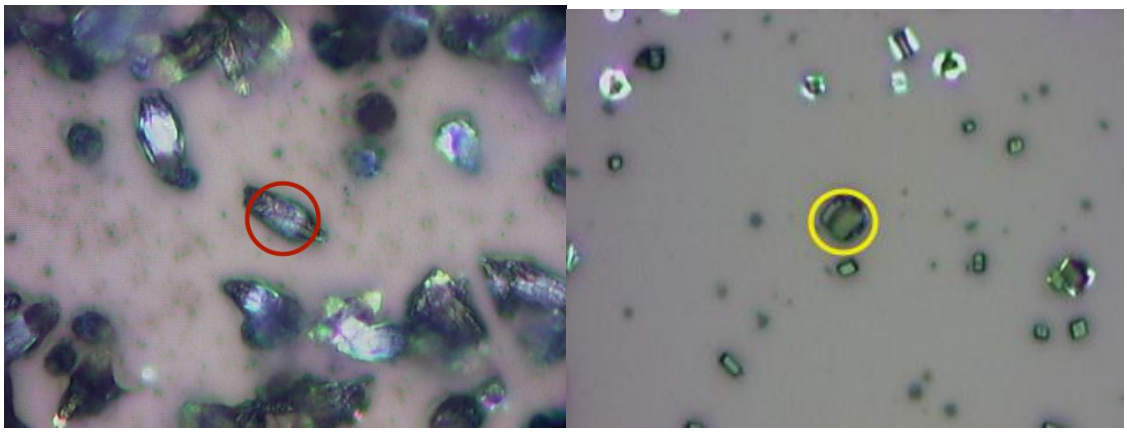

Figure 6: The red circle shows where the Raman laser was aimed for the experimental aragonite spectrum and the yellow circle shows where the Raman laser was aimed for the experimental calcite spectrum.

Time-Lapse Photography:

In order to find the nucleation rates, a computer-controlled Nikon microscope was used to capture time-lapse photography of the calcium carbonate nucleation occurring. A polarizing filter is added to the microscope as the nuclei bend light in various angles other than the normal light pattern thus causing the nuclei to stand out in a black background. A Nikon camera is attached to the microscope and controlled by a computer with NVIDIA software. This software is capable of time-lapse photography over a set time and frequency. A select number of the pictures are taken from the series and analyzed by hand counting. Each picture is broken up into six sections and two sections are picked are random and all of the nuclei are counted and averaged.

After the nuclei are counted from the select pictures, the number of nuclei are graphed against the time lapsed to produce plots of number of nuclei versus time elapsed (Figure 9), for which the slopes are nucleation rates. The nucleation rates are found by using a linear regression model on the portion of the graph where the numbers of nuclei forming are increasing at steady state. The rest is left out because the space left for nucleation on the slide is insufficient for the sustained nucleation rate. Slope of each of those regressions provides a rate of nucleation for each of the saturation states or Ω values from each experimental run. The points from each saturation state are then plotted and an exponential regression is run on the data.

Results:

A time-lapse series was taken for each experimental run for the different saturation states using the same 200x magnification. Figures 7 and 8 are photos from two of the experimental runs and show the nuclei on the top glass microscope slide. The nucleation is not always uniform densities in the viewing area, which is why each picture is separated into six sections and two sections are picked at random, counted and averaged. For each of the saturation states, eight pictures were selected in the time-lapse at critical and regular intervals to provide the data. The numbers of nuclei are plotted over time for each saturation state to show the nucleation rates for each saturation states. (See figure 9) A linear regression is run for each saturation state where the number of nuclei are increasing at a constant rate to get the nucleation rate for that saturation state. Plotting the nucleation rate for each saturation state or Ω reveals a sharp exponential relationship. (See figure 10)

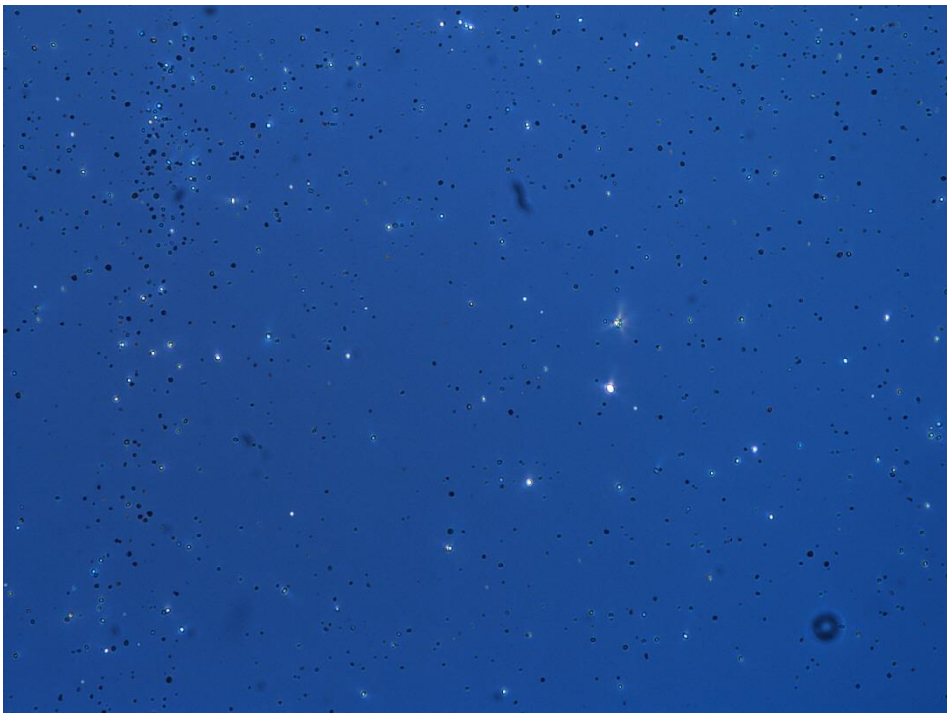

Figure 7: Image from a time-lapse series of calcite nucleation in a 0.3468mm^2 area with a saturation state of Ω=7.5 after 72 minutes. Each point represents a nucleus that is growing.

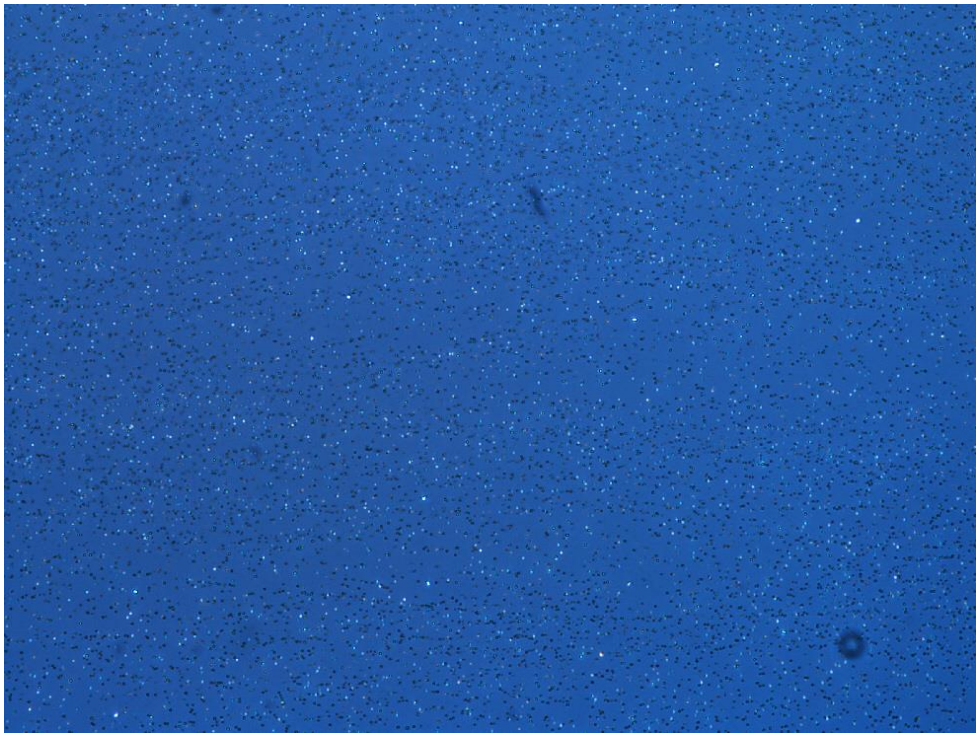

Figure 8: Image from time-lapse series of calcite nucleation in a 0.3468mm^2 area with a saturation state of Ω=9.2 after 40 minutes. Each point represents a nucleus that is growing.

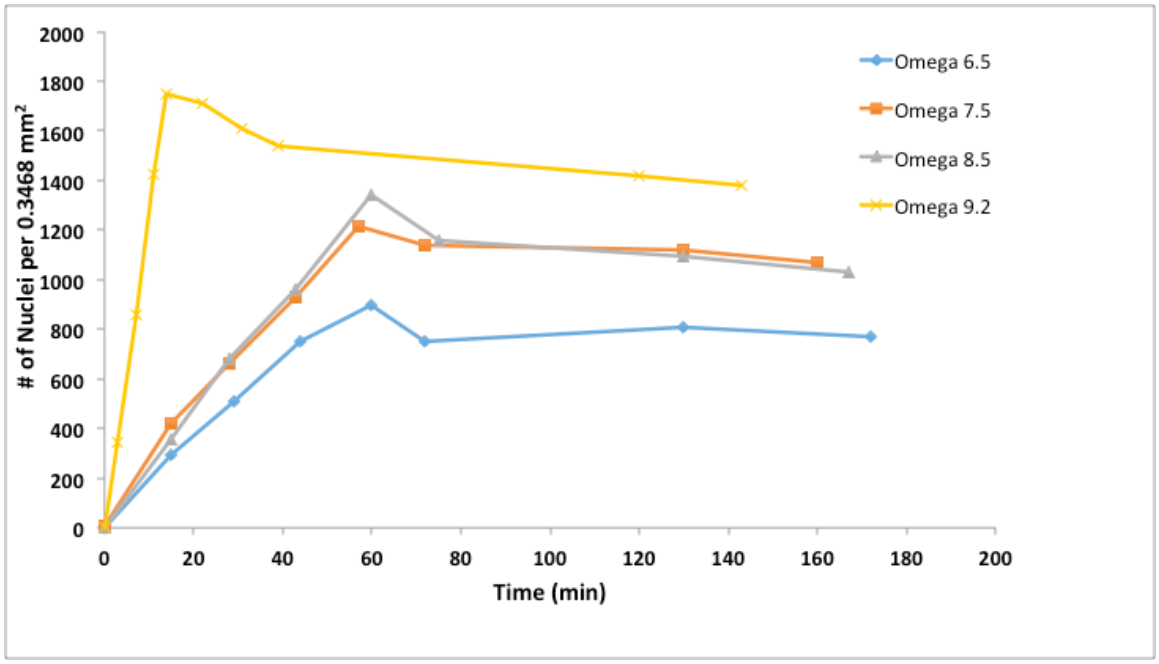

Figure 9: Calcite nucleation rates for four different saturation states.

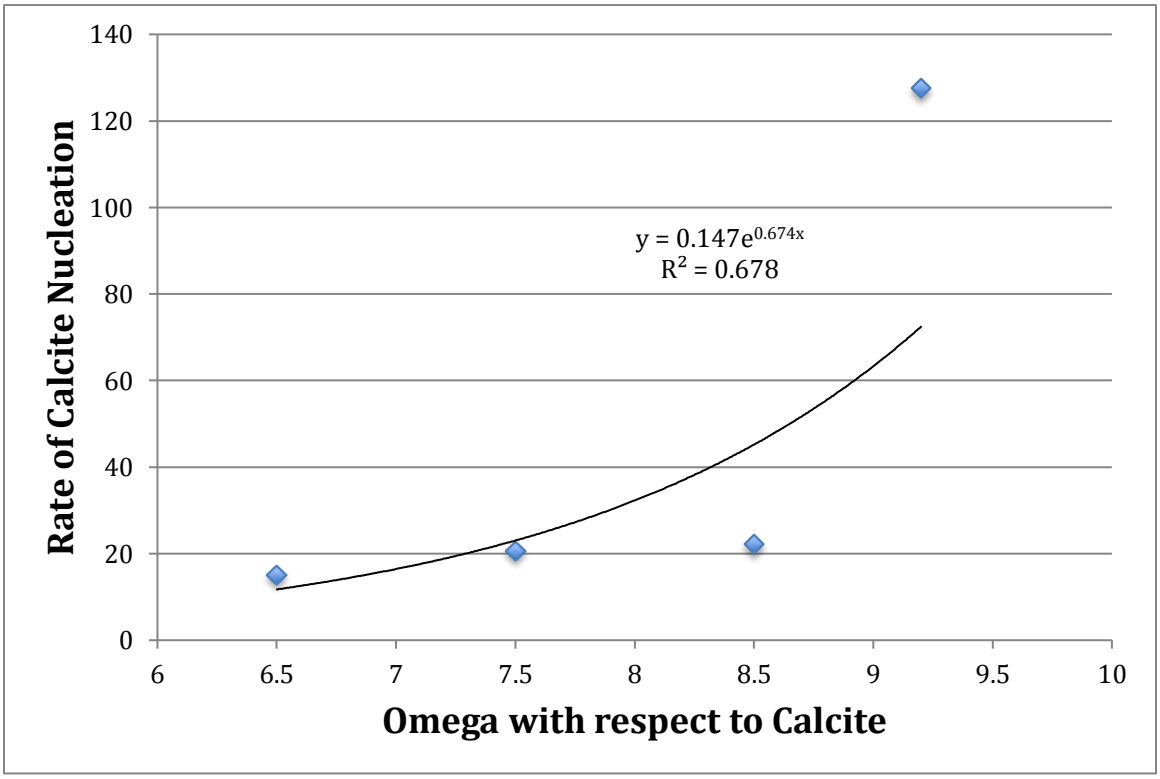

Figure 10: Change in calcification rates by changing saturation states.

Discussion:

This study indicates how saturation states change nucleation rates of calcium carbonate with respect to the classical nucleation theory. As mentioned previously, the classical nucleation theory is the combination of the factors that influence nucleation that gives a nucleation rate. Two major factors that affect nucleation rates are the saturation state and interfacial surface energy between the nucleus and the glass microscope slide as well as the solution. In this experiment, the effect of saturation state on nucleation rate of calcite was investigated. The slope of the nucleation rate versus the saturation state demonstrates the sensitivity of the calcium carbonate nucleation to saturation state without the influence of biology altering the interfacial energies between the solution and solid. As shown above in Figure 9, there is a steep drop in nucleation rates as saturation states decrease. This is significant because this would imply that there is a threshold saturation state for nucleation. If the calcifying fluid Ω drops below this threshold, marine calcifiers could have to expend much more energy when using the proton pumps to manipulate their calcifying fluid for nucleation and will have to adapt to slower growth rates, which could impact their fitness.

More analysis of the results gives us the proportionality constants from the classical nucleation theory. Manipulating the standard nucleation equation (4) by taking the natural log of both sides, we can fit the data into a linear format with equation 5. For the standard mineralization equation (4), recognize that σ is the natural log of Ω, A and β are proportionality constants, and α^3 accounts for the

interfacial energy. By taking the natural log of the nucleation rates and plotting them against the inverse of the natural log of the saturation state squared, we can find a linear plot where the slope and y-intercept have valuable meanings.

$$\text{Eq 4: } Rate = J = Ae^{\frac{-\beta\alpha^3}{\sigma^2}}$$

$$\text{Eq 5: } \ln(\text{J}) = -\beta\alpha^3\left(\frac{1}{\sigma^2}\right) + \ln(A)$$

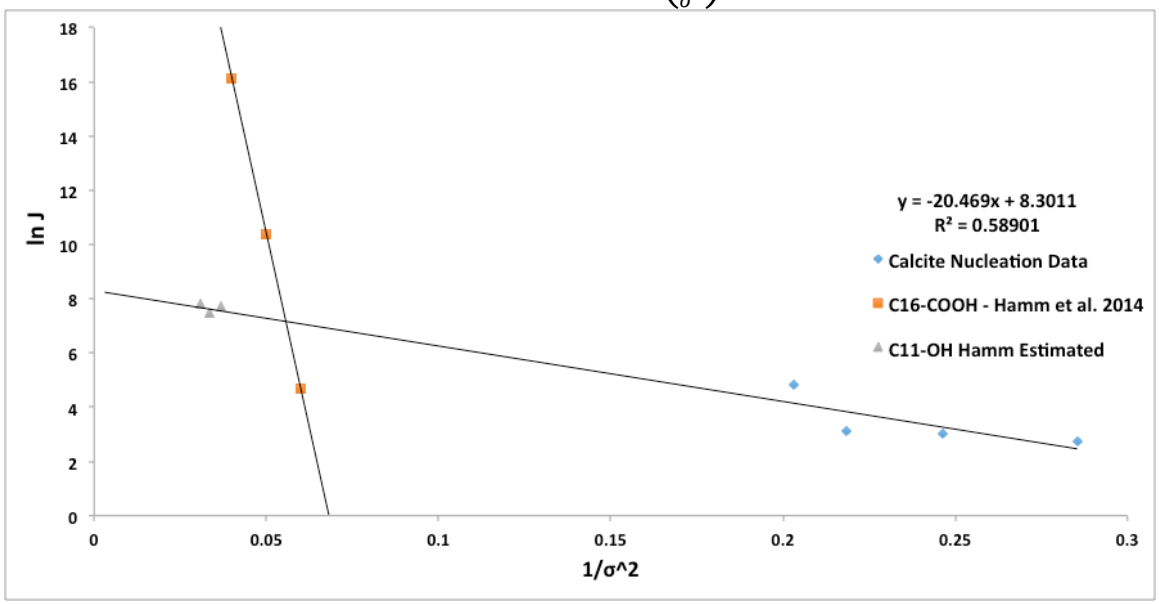

Figure 11: Graph of relationship between nucleation rates (ln J) and the saturation states ($1/(\ln \Omega)^2$). Data from the nucleation work by Hamm et al. (2014) is added to the plot. The orange squares are nucleation rates from a surface coated with C16-COOH and the gray triangles are nucleation rates from a surface coated with C11-OH.

Interpreting the data within the bounds of the standard nucleation equation gives a linear graph relating the nucleation rates and saturation states. The slope of the data from this experiment, -20.469, is $-\beta\alpha^3$ and reveals something about the interfacial energy. The y-intercept of the plot is *ln* A and using simple algebra, we determined the proportionality constant A is equal to 4028.3. This number represents J_{max} or the maximum nucleation rate if there is an infinitely high

saturation state. This constant is indicative of molecular motion during nucleation and describes what frequency the ions are colliding in solution and forming nuclei.

As shown in Figure 11, although the organic surfaces from Hamm et al. (2014) can increase nucleation rates at a high saturation state, they will be much more sensitive to ocean acidification that a simple C11-OH surface. We can also assume that if these surfaces follow Classical Nucleation Theory, then below an omega of about 75, calcite nucleation will be inhibited by the surface relative to the C11-OH surface. This could be used in an organism as a way to increase the saturation state until amorphous calcium carbonate can form.

Another unusual result is that there is a reduction in number of nuclei after a large nucleation spike. It is unclear what causes this to happen. One possibility is that the nuclei are dissolving and reforming as a more stable polymorph or helping another nuclei grow. Another possibility could be that the nuclei are falling off the slide by the flow rate.

It is also interesting to compare the nucleation rate to the crystal growth rate. The nucleation rate increases exponentially faster than the crystal growth rate and thus produces a bottleneck effect where as long as nucleation occurs, the structure can grow. In either case, the saturation state has a significant impact on the nucleation rates.

These results lead to further questions about how interfacial energies could be manipulated to allow for lower energy barriers and lower saturation states necessary for calcium carbonate nucleation. For example, one could inhibit growth through increasing the energetic barrier, and then nucleation should preferentially

occur in another area. Another option is to use organics to reduce the interfacial surface energies to allow for faster nucleation rates on that surface. Finally, it would be ideal to use the same technique to look at aragonite nucleation rates to directly compare to the calcite nucleation rates. It would also allow scientists to see how marine calcifiers will react to future acidic ocean conditions.

References:

Al-Horani, F.A., Al-Moghrabi, S.M. & de Beer, D. (2003). The mechanism of calcification and its relation to photosynthesis and respiration in the scleractinian coral Galaxea fascicularis. Mar. Biol. 142:419-426.

Allemand, D., Ferrier-Pagès, C., Furla, P., Houlbrèque, F., Puverel, S., Reynaud, S., Tambutté, E., Tambutté, S., Zoccola, D. (2004). Biomineralization in reef-building corals: from molecular mechanisms to environmental control. C. R. Palevol 3:453-467.

Berner, R.A. (1975). The role of magnesium in the crystal growth of calcite and aragonite from sea water. *Geochimica et Cosmochimica Acta.* 39:4 489-494.

Cai, W-J., Ma, Y., Hopkinson, B.M., Grottoli, A.G., Warner, M.E., Ding, Q., Hu, X., Yuan, X., Schoepf, V., Xu, H.,, Han, C., Melman, T.F., Hoadley, K.D., Pettay, D.T., Matsui, Y., Baumann, J.H., Levas, S., Ying, Y., Wang, Y. (2016). Microelectrode characterization of coral daytime interior pH and carbonate chemistry. *Nat. Commun.* 7:11144.

Costanza et al. (1997). The value of the world's ecosystem services and natural capital. *Nature* 387: 253-260.

Crutzen P.J. (1992). Ultraviolet on the increase*. Nature.* 356:104-105.

Doney, S.C. (2010). The growing human footprint on coastal and open-ocean biogeochemistry. *Science.* 328:1512-1516.

Doney, S.C., Fabry, V.J., Feely, R.A., Kleypas, J.A. (2009). Ocean Acidification: The Other CO_2 Problem. *Annual Reviews.* 1: 169-192.

Doney, S.C., Ruckelshaus, M., Duffy, J.E., Barry, J.P., Chan, F., English, C.A., Galindo, H.M., Grebmeier, J.M., Hollowed, A.B., Knowlton, N., Polovina, J., Rabalais, N.N., Sydeman, W.J., Talley, L.D. (2012). Climate change impacts on marine ecosystems. *Ann. Rev. of Mar. Sci.* 4:11-37.

De Yoreo, J.J., Vekilov, P.G. (2003). Principles of Crystal Nucleation and Growth. *Reviews in Mineralogy and Geochemistry.* 3: 57-93.

Gladfelter, E.H. (1982). Skeletal Development in *Acropora cervicornis*: I. Patterns of Calcium Carbonate Accretionn in the Axial Corallite. *Coral Reefs*. 1: 45-51.

Hamm, F. M., Giuffre, A. J., Han, N., Tao, J., Wang, D., De Yoreo, J. J., & Dove, P. M.

(2014). Reconciling desparate views of template-directed nucleation through measurement of calcite nucleation kinetics and binding energies. PNAS, 111
Hoegh-Guldberg, O. & Bruno, J.F. (2010). The impact of climate change on the world's marine ecosystems. *Science.* 328: 1523-1528.
Hu, Q., Nielsen, M. H., Freeman, C. L., Hamm, L. M., Tao, J., Lee, J. R. I., Han, T.Y.J., Becker, U., Harding, J. H., Dove, P. M., & De Yoreo, J. J. (2012). The thermodynamics of calcite nucleation at organic interfaces: Classical vs. non-classical pathways. *Faraday Discussions.* 159: 509-523.
IPCC. (2014). Climate Change 2013. The Physical Science Basis. Contribution of Working Group I to the Fifth Assessment Report of the Intergovernmental Panel on Climate Change
Johns et al. (2001). Socioeconomic study of reefs in southeast Florida. Report by Hazen and Sawyer under contract to Broward County, Florida. 225 pp.
Jameson, S.C, McManus, J.W., Spalding, M.D. (1995). State of the Reefs: Regional and Global Perspectives. Washington, D.C., ICRI., U.S. Department of State.
Meldrum, F.C. (2003). Calcium carbonate in biomineralisation and biomimetic chemistry. *International materials reviews.* 48:3 187-224.
Orr JC, Fabry VJ, Aumont O, Bopp L, Doney SC, et al. (2005). Anthropogenic ocean acidification over the twenty-first century and its impact on calcifying organisms. *Nature* 437:681–86
Pandolfi, J.M., Connolly, S.R., Marshall, D. J., Cohen, A.L. (2011). Projecting coral reef futures under global warming and ocean acidification. Science. 333:418-422.
Ries, J.B. (2011). A physicochemical framework for interpreting the biological calcification response to CO_2-induced ocean acidification. *Geochim. Cosmochim. Acta.* 75:4053-4064
Sabine CL, Feely RA, Gruber N, Key RM, Lee K, et al. (2004). The oceanic sink for anthropogenic CO2. *Science* 305:367–71
Sabine CL, Feely RA. (2007). The oceanic sink for carbon dioxide. In *Greenhouse Gas Sinks*, ed. D Reay, N Hewitt, J Grace, K Smith, pp. 31–49. Oxfordshire: CABI Publishing
Venn, A.A., Tambutté, E., Holcomb, M., Laurent, J., Allemand, D., Tambutté, S. (2012). Impact of seawater acidification on pH at the tissue-skeleton interface and calcification in reef corals. *PNAS.* 110:5 1634-1639.
Wallace, A. F., DeYoreo, J. J., & Dove, P. M. (2009). Kinetics of silica nucleation on carboxyl-and amine- terminated surfaces: insights for biomineralization. *Journal of the American Chemical Society*. 131:14 5244-5250.